Arab American University-Jenin

Faculty of Graduate Studies

Impedance Spectroscopy and Temperature Dependent Structural Properties of La-Doped $Bi_{1.5}Zn_{0.92}Nb_{1.5}O_{6.92}$ Pyrochlore Ceramics

By

Qotiabah A. A. Alkarem

Supervisor:

Assoc. Prof. Dr. Adli Saleh

Co. Supervisor:

Assoc. Prof. Dr. Hazem Khanfar

This thesis was submitted in partial fulfillment of the requirements for

The Master's degree in Physics

September/2017

Impedance Spectroscopy and Temperature Dependent Structural Properties of La-Doped $Bi_{1.5}Zn_{0.92}Nb_{1.5}O_{6.92}$ Pyrochlore Ceramics

By

Qotiabah A. A. Alkarem

This thesis was defended successfully on September 16th 2017 and approved by:

Committee members	Signature
1. Assoc. Prof. Adli Saleh/ Supervisor	……
2. Assoc. Prof. Hazem Khanfar/ Co. Supervisor	……
3. Prof. Atef Qasrawi/Internal Examiner	……
4. Prof. Ghassan Saffarini/External Examiner	……

Declaration

I hereby declare that this thesis, submitted for the degree of master of science in physics, is the result of my own research, except where otherwise acknowledged, and that it has not been submitted, in whole or in part, in any previous application for a degree to any other university or institution.

Signed:

Qotiabah A. A. Alkarem

Date:

E-mail: qotiabah2012@gmail.com

Dedication

I dedicate this work to the souls of the martyrs of our nation who sacrificed their pure blood for the elevation of the word of God and the liberation of Palestine; to our brave captives in the occupation prisons who sacrificed their youth for the Palestine cause; to the springs of love and tender my mother and father; to the beautiful roses to my friends; to my love, to my brothers Nael, Sajed and Naser and sisters Asmaa, Somaya and Ruba. In addition, to all who have enlightened me by the way of science and education.

Acknowledgments

In the name of Allah, the most gratious and the most Merciful, for granting me the ability and the courage to accomplish this work.

I would like to express my profound gratitude to my research advisors, Assoc. Prof. Dr. Adli Saleh and Assoc. Prof. Dr. Hazem Khanfer for their guidance, patience and continuous support through all stages of this work. I would like also to extend my thanks to the faculty and staff of the physics department for their help and support during my graduate work. Particularly, I would like to thank Prof. Dr. Attef Qasrawi for his support. I would also like thank to my colleagues who have always worked to help and support me to accomplish this work. Finally, big thanks you to my parents, brothers and sisters. In particular, I would like to thank my mother who always supported me whenever I felt weak until I managed to accomplish this work.

Impedance Spectroscopy and Temperature Dependent Structural Properties of La-Doped $Bi_{1.5}Zn_{0.92}Nb_{1.5}O_{6.92}$ Pyrochlore Ceramics

By

Qotiabah A. A. Alkarem

Supervisor:

Assoc. Prof. Dr. Adli Saleh

Co. Supervisor:

Assoc. Prof. Dr. Hazem Khanfar

Abstract

In this work, we explored some smart properties of the lanthanum doped $Bi_{1.5-X}La_XZn_{0.92}Nb_{1.5}O_{6.92}$ (La-BZN) pyrochlore ceramics. This was done because there are known applications for BZN high dielectric material. In this study, the La content denoted by (X) was varied in the range from 0.10 to 0.22. By increasing the La content from 0.10 to 0.20, a single phase appeared where the grain sizes increased from 33 to 57 nm respectively. Also, we explored temperature effects on the structural properties of the La-BZN in the temperature range of 298 to 470 $^{\circ}$K using the X-ray diffraction technique (XRD) for two samples with X= 0.10 and X= 0.20. The temperature dependent XRD analysis was employed to determine the temperature effects on the lattice constant, grain size, micro strain, dislocation density and degree of orientation. By increasing temperature from 298 to 390 $^{\circ}$K, the strain, the dislocation density and lattice constant increased for both samples, while the grain size decreased in the same temperature range. In addition, the room temperature impedance spectrum was recorded in the frequency range from 10 to 1800 MHz. Physical parameters of capacitance, conductance, reflection coefficient, return loss and voltage standing wave ratio that are needed for using the La-BZN as an active

resonator in telecommunication technology were investigated. These measurements provided information about the doping effects on the dielectric properties in this frequency range. The capacitance increased from 13.5 to 20.6 pF as the doping ratio increased from X= 0.10 to X= 0.22. The dielectric constant increased in the doping ratio range of X= 0.10 to X= 0.20 from 31 to 55.

Keywords: BZN, dielectric, mechanical, strain, impedance, return loss

List of contents

List of tables

List of figures

Chapter One

Introduction and Literature survey

Ceramic is a Greek word whose origin is "KERAMICOS" meaning burnt stuff, which are compounds between metallic and non-metallic elements often associated with ionic bond and sometimes combination of ionic and covalent bonds. The ceramic materials are divided into two types: traditional ceramics and new ceramics. Traditional ceramics are made from minerals occurring in nature such as clay, tiles and bricks, while new ceramics are made from synthetically produced raw materials such as Alumina (Al_2O_3) and Titanium Carbide (TiC). Ceramics are composed of electrically charge ions known as cations and anions. The cations are positively charged and are metallic ions, while the anions are negatively charged and are non-metallic. The cations are usually smaller than the anions so, the ratio between the radius of the cation to the radius of the anion is less than one ($r_C / r_A < 1$) and each cation is surrounded by a group of anions. When the anions surrounded by the cations are all connected to this cation, the crystal structure of the ceramic is stable as shown in Fig1.1.

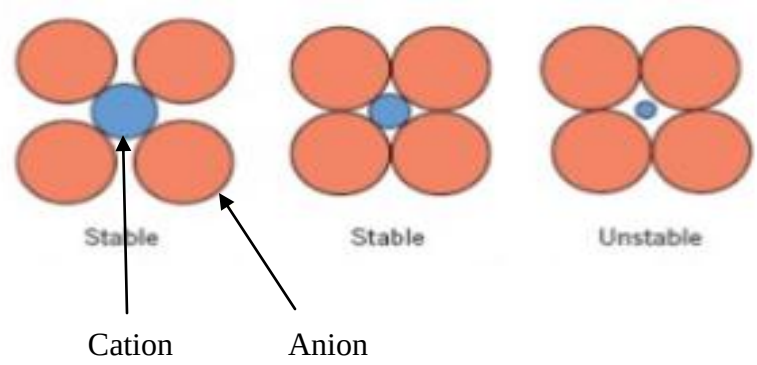

Fig1.1.: Stable and unstable of ceramic crystal structure

Ceramics poses some important properties such as thermal stability, brittle, hardness and wear resistance which makes them candidate for many applications such as electronic and aerospace industries.

Pyrochlore ceramics compounds related to flurite structure BO_2 that has face centered cubic (FCC) crystal structure [1]. The formation of A2B2X6Z and A2B2X7 ceramics include A and B metallic atoms at cation sites while X and Z at anion sites. As the Fig. 1.2 (a) shows the A cations are at 16 d and B anions at 16 c, the X anions are at 48 f and the Z anions are at 8 b. In the pyrochlore, the A cation have coordination number of 8, while B exhibit coordination number of 6. In the pyrochlore, to reveal stable formation for ions $^{+}3$, $^{+}4$, and for ions $^{+}2$, $^{+}5$, the ionic radius ratio ($r_A/r_{B)}$ must be located between $1.46 < r_A/r_B < 1.80$, $1.40 < r_A/r_B < 2.20$ respectively [2]. In the past few years there has been a great interest in researching the applicability of ceramics as high frequency dielectric, such as Ba-Nd-Ti-O and Bi-Zn-Nb-O systems. Bismuth-based pyrochlore exhibit well known high frequency dielectric with useful properties for multi- layer capacitor [1].

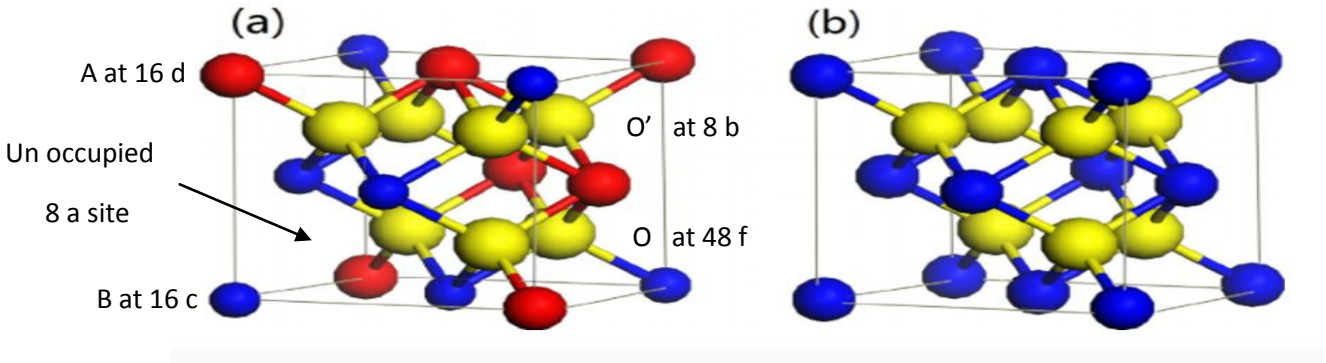

Fig.1.2: (a) pyrochlore crystal structure. (b) Fluorite crystal structure.

The bismuth-zinc-niobium (BZN) with stoichiometry $Bi_{1.5}Zn_{0.92}Nb_{1.5}O_{6.92}$ is the base of pyrochlore ceramics which has been studied since late of nineteenth century when the chinese researchers reported it for the first time [1]. It is considered an important compound in a Class-I dielectric group this material as BZN cubic pyrochlore [3]. The BZN has many characteristics such as high dielectric constant, low dielectric loss which led to reduce the size of microelectronic circuits [1-4], whereas relative dielectric permittivity and electrical resistivity are high [5]. These properties make combined with thermal stability and low sintering temperature of about 1000 C˚ [6], BZN, as previously mentioned, useful in different applications. A good example is electromagnetic energy storing devices which makes these types of ceramics attractive to produce many electronic devices like complementary metal-oxide-semiconductor (CMOS) capacitor [7], very high tunable inter-digital capacitor (IDC) [8], and promising material for microelectronic industry as multilayer capacitor as resonators [3]. Reports on the properties of BZN pyrochlore ceramics had shown their wide applicability in concurrent technology. Recently, a low-voltage (less than two volts) organic transistors and depletion-load inverters are fabricated using a 200-nm-thick gate dielectric using the BZN pyrochlore [9]. These inverters are reported to be successfully running with excellent noise margins. In addition, gigahertz centered microwave filters based on BZN ceramics is reported to exhibit novel characteristics that make them attractive for applications which acquire high frequency devices [10]. Moreover, make BZN ceramics are reported to exhibit negative capacitance (NC) spectrum in the frequency range of 22-210 MHz. The NC effect displays wide tunability at 50 and 150 MHz. Such features are interesting as they allow the cancellation of the positive parasitic capacitance in electronic circuits [11]. There is a

significant volume of research reported in the scientific literature which aim to improve the physical properties of pyrochlores [12]. For example, increasing the yttrium doping content from 0.04 to 0.07 in the BZN shrunk the optical energy band gap from 3.60 to 2.75 eVs, respectively [8]. In addition, the doping of MgO into the pyrochlore displayed typical dielectric relaxation behavior with strong frequency dispersion at low-temperature [13]. The indium and iridium doping into BZN pyrochlore altered the relative permittivity of the BZN ceramics. Namely, the relative permittivity of Ir doped BZN slightly decreased with Ir content. However, In doping into the BZN decreased the relative permittivity at low doping ratios, but increased it at high doping ratios [14]. The tantalum doping into BZN pyrochlore, the dielectric constant decreased and electrical conductivity increased as doping of Ta increased from 0.20 to 1.50 [3]. Also, the nickel affected the optical and electrical properties of BZN pyrochlore and altered the energy gap from 3.30 eV to 3.52 eV and the temperature dependent electrical resistivity increased with increasing Ni content from 0.00 to 0.10 [15]. The lanthanum (La) is a commonly used element in nature, with many physical properties such as melting point of about 920 C and the boiling point of about 3469 C. The structural type of La is hexagonal with lattice parameters a= 3.772 A and c= 12.144 A at room temperature and it is an element of P63/mmc space group. In this work, we will investigate the effects associated with the lanthanum substitution into the pyrochlore. Particularly, the La content effects on the structural and electrical properties as a function of doping content. The temperature effects on the structural and electrical parameters will also be examined to investigate the micro strain of the structure of the doped BZN pyrochlores.

Chapter Two
Theoretical Background

Ceramics are one of the oldest materials dating back to the dawn of human civilization, which are inorganic and non-metallic materials and often polycrystalline materials. They can be formed at room temperature from a group of raw materials and possible to obtain their typical characteristics by sintering at high temperatures. There are several methods used in the preparation of ceramics that will be identified in this chapter.

2.1 Ceramics synthesis:

Ceramics are commonly used materials. There are different ways in preparing the powder used so far have been classified into two groups are break-down process and build-up process. The break-down process is division of large particles is ground into very small pieces (< 1μm). The build –up process it is the reverse of the break-down process, so that it is produced a particle by precipitation and deposition. The build-up processes including several methods. Solid –phases synthesis including solid-solid reaction (solid solution) and solid-vapor reaction. Liquid -phase synthesis including precipitation, hydrolysis (sol-gel process) and solvent evaporation. Vapor -phase synthesis including chemical vapor and physical vapor depositions [16]. The solid steady state methods can operate by several mechanisms, such as diffusion and chemical reactions, so that the diffusion in ceramics is always ionic in nature and depend on electron conductivity by the presence of chemical reactions. The sol is a colloidal particles or polymers in the solvent (particles in a liquid); it results in being a gel, this is the sol-gel method. Through the sol-gel method we can get

crystal particles or amorphous structure. If the particles are colloidal and the solvent was alcohol or water, the particle repulsion prevented the agglomeration and consist the gel from electrostatic effect and we get the crystal particle. But, if the particles are polymers and the solvent is alcohol, the agglomeration prevented by small size and the gel was formed from the polymerization and in the result, we get the amorphous structure. In this study, we used solid-solid reaction to prepare the BZN ceramics [16].

2.2 Applications of ceramics:

Throughout the ages there have been many factors that have played an important role in determining the competitiveness of individuals and communities. As the days passed, the identification of material structure and the deepening of understanding of atomic and micro structure became important for improving existing materials and developing new materials to meet the important needs of industrial and social challenges in today's competitive world. Ceramic technology has played an important role in this regard, especially in technological advances in many industrial sectors. It is worth mentioning that this technological progress occurs in a very competitive environment as the resources required are limited and the need for raw materials is very important throughout the ages. Over time, technology has become better and material information has increased. Composite ceramic materials played an important role during technological development, especially metal technology, to withstand very high temperatures. This continued until the 1970s when mineral impact was reduced by the application of engineering polymers and their compounds. With the increasing sophistication and practical uses of engineering, the volume of ceramic production such as bricks, cement and tiles has increased significantly.

When the volume of production reached a maximum extent, these materials were gradually replaced by engineering plastics. At the same time, the use of advanced materials began to rise, including advanced ceramics [17]. Classical ceramics are classified into three main groups of sensu strictu, glasses and hydraulic adhesives. These groups are characterized by temperature, processing steps and time of invention. As mentioned previously, the need for raw materials is significant and important in the ceramic industry [17]. The raw materials used in the production of ceramics made of silicate have been divided into three types of high plastic materials such as clay, sparingly plastic and non-plastic materials. Clay is one of the most famous examples of ceramics. It is a product of feldspars, micas and other rocks that form rock. Therefore, they are mechanical mixtures of very different components. These mixtures consist of four main components: fine-grained weathering, newly formed clay minerals, the residues of organisms and the neoformations that occur after deposition. The importance of clay is one of the most important raw materials for classical ceramics and its chemical and structural volatility. The advanced ceramics have been classified into structural advanced ceramic and functional advanced ceramics. Advanced structural ceramics are used when a system component is subjected to high mechanical, thermal or chemical loads. The structural ceramic model is alumina, zirconia, cordierite, mullite, spinel, silicon nitride, silicon carbide, boron nitride, titanium nitride and titanium pore. While functional advanced ceramics are in contrast to structural ceramics, where microscopic effects are used inside the size or on ceramic surfaces. These effects include semiconductors, pyroelectric and superconducting properties. Over time, ceramic production has increased and new applications have emerged and are increasing in emerging applications in the field of ceramic nanotechnology. It is clear that structural

ceramics are experiencing strong growth due to the increasing demand for ceramic shields for personal protection and military vehicles. While electronic ceramics are a mature market, some of its sectors are also growing strongly, such as solid and soft magnets, and semiconductor packages. Oxidized ceramic materials have played a prominent role in having important properties that led to important modern applications such as sensors, capacitors, optoelectronic shutters and superconductors. Dielectric materials are divided into three sections according to their physical effects. Normal dielectric materials, which are subject to polarization due to their response to an external electric field. Pyroelectrics materials are substances that are subject to polarization by temperature gradient. There are two types of these materials. Ferroelectricity materials which can be reversed by the application of an external electric field and the ferroelasticity material, which can be changed in the direction of automatic polarization by application of mechanical stress. The third type of dielectric materials are the Piezoelectrics, which works on mechanical stress to attract these materials. The basic requirement of these materials for polarization is the lack of crystal structure to the center of symmetry. Ferroelectric and piezoelectric ceramics play a prominent and important role in electrical and electronic applications such as multilayer capacitor, dielectric resonators and low - insertion loss bandpass filters for microwave communication components. Ceramic and most polymeric materials are dielectrics in which the electrons are constrained and cannot move freely with an external electric field so that there is no long-range transport of charge carriers but only the displacement of electrons, ions or dipoles.

2.3 Polarization and dipole moment:

The degree of displacement depends on the intensity of the external electric field. When both positive and negative charges are arranged in two different directions, the crystal has dipole moment. Thus, the polarization is the macroscopic dipole moment per unit volume and given by

$$P = \varepsilon_{\circ} \chi E \quad (3.1)$$

where P is a dipole moment, $\varepsilon_{\circ}$ is a dielectric permittivity of the vacuum, χ is the dielectric susceptibility and E is the macroscopic electric field strength in the dielectric.

The dielectric displacement vector is defined as

$$D = \varepsilon E = \varepsilon_{\circ} E + P \quad (3.2)$$

and ε_r is the relative dielectric permittivity

$$\varepsilon_r = \varepsilon/\varepsilon_{\circ} \quad (3.3)$$

The dielectric and electromechanical coupling properties of ceramics are dependent on three factors the dielectric permittivity (ε), quality factor (Q) and the temperature coefficients of both resonance frequency and dielectric permittivity. Accordingly, the desired ceramic should have high dielectric constant leads to a miniaturization of the device, high quality factor; that's a law dielectric loss and a zero temperature coefficient of the resonance frequency to attain temperature stability of the device [17].

The important characteristics of the ceramics mentioned earlier depend on the fact that the pyrochlore crystal structure allows for a wide range of ion substitutes in both sites A and B and these compounds can accommodate various cations at these sites and for their large

stability field that convey different properties to the pyrochlore. On the other hand, there is another factor that makes ceramics especially BZN possess these characteristics is a low sintering temperature (less than 1000 C°) [3].

2.4 Characterization techniques:

X-ray diffraction, impedance spectroscopy analysis and electrical conductivity by thermionic emission were used to investigate the physical properties of the doped samples of La-BZN.

2..4.1 X-Ray diffraction:

X-rays are electromagnetic waves with a range of 0.10 -100 A°. It is known that the distance between the atoms in the material is very small (a few angstrom), so the X-ray` with a few angstroms wavelengths is important technique and accurate in the identification of the internal structure of materials. When a beam of X-rays falls on the material, the waves emitted by the atoms are in the phase with each other in the direction of the observer [18].

X-rays are produced using an evacuated tube of air containing a cathode that acts as a source of electrons connected to voltage difference to heat it and emit the electrons. These electrons are accelerated through a high potential difference (few tens of KV) towards a material anode which emits the X-ray with Kα radiation of a copper anode of average wavelength 1.5405 A. The path difference between two rays is 2dsinθ as shown in Fig.2.1 for constructive interference [19].

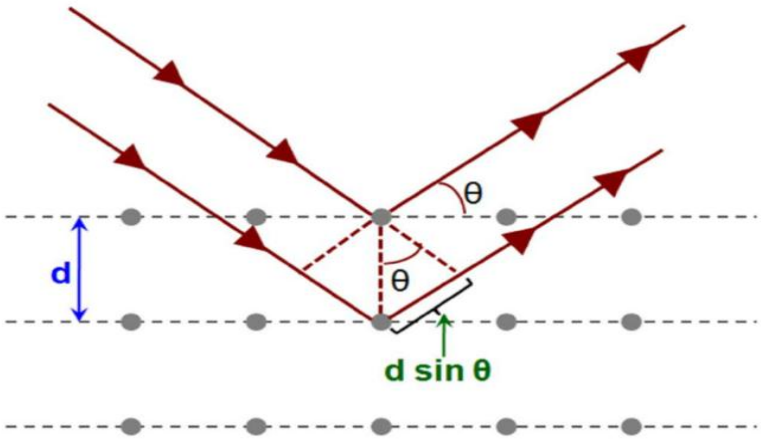

Fig.2.1: Bragg condition

$$2\,d\,\mathrm{Sin}\,\theta = n\,\lambda \qquad (3.4)$$

This is Bragg condition for constructive interference where, (d) is the inter-planer spacing, (θ) is the angle of incidence and (n) is the order of corresponding diffraction. The solid-state physics divided to non-crystalline (or amorphous) that atoms was random arrangement and crystalline that divided to single crystal and polycrystalline, the difference between them is a grain size. In the single crystal, the grain is only one and no grain boundaries, but in the polycrystalline the grain is more than one and contains on grain boundaries. The grain sizes we can calculate from Scherer equation [20]

$$D = (0.94 \times \lambda) / (\beta \times \mathrm{Cos}\,\theta) \qquad (3.5)$$

Where (D) is the grain size, (λ) is wavelength, (β) is the Line broadening and (θ) is incident angle. The strain is the ratio between the changes in the bond length to the original bond length which may be calculated from strain equation [21]

$$\varepsilon = (0.94 \times \lambda) / (4 \times D \times \sin\theta) \quad (3.6)$$

Where (ε) is the strain, (λ), (D) and (θ) are the same in the equation (2).

The dislocation density defined as the number of lines per cm^2 and expresses the degree of cohesion of atoms of the material between them and increase with the strain increase. When the value of dislocation density is small, the material is good. We can calculate it's from least square method [21]

$$\delta = (15 \times \varepsilon) / (a \times D) \quad (3.7)$$

Where (δ) is the dislocation density, (ε) is the strain, (a) is the lattice constant and (D) is the grain size.

2.4.2 RLC circuit:

The RLC circuit is an electric circuit that contains resistance R, inductor L and capacitance C connected in series as shown in Fig.2.2.

The impedance is the opposition shown by the circuit to pass the current when applying a voltage [22]

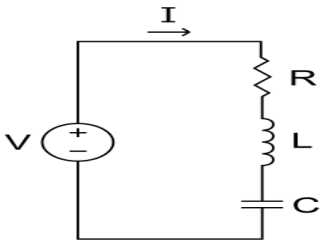

Fig.2.2: RLC sires circuit

$$|Z| = (R^2 + X^2)^{1/2} \quad (3.8)$$

Where (Z) is the impedance, (R) is the resistance and (X) is reactive component of Z which we can calculate from the following equation

$$X = (-1/ 2\pi fC) + 2\pi fL \quad (3.9)$$

Where (C) is the capacitance and (L) is the inductance.

The admittance is that express the extent to which the circuit can pass the current [23].

$$Y = G + i\,B \qquad (3.10)$$

Where (B) is the imaginary part and (G) is the real part they represent the conductivity which we can calculate from following equation

$$G = R / (R^2 + X^2) \qquad (3.11)$$

The dielectric constant is the ability of material to store the electrical energy in an electric field. We can calculate from the following equation

$$C = k (\varepsilon_0 A / d) \qquad (3.12)$$

Where (C) is the capacitance, (k) is the dielectric constant, (A) is the area of the sample and (d) is the distance between two electrodes.

2.4.3 Electrical conductivity by thermionic emission:

Electric conductivity is one of the most delicate physical properties to characterize in insulating material. Electrical conductivity measurements in dielectric materials is done as a function of temperature. The electric conductivity as a function of temperature can be calculated from Arrhenius equation as follow [24].

$$\sigma = \sigma_0 \exp (-Ea / kT) \qquad (3.13)$$

Where (σ_0) is the preexponential factor, (k) is the Boltzman constant, (T) is the temperature and Ea is the activation energy.

Chapter Three
Experimental Details

3.1 Sample preparation:

Our samples which were prepared at Marmara University, were prepared by solid state reaction method. In that method, Bi_2O_3, ZnO and Nb_2O_3 were mixed with Lanthanum (La) in ethanol for 15 hrs. The sample was then dried at 100 C^o for one day, after that it was calcinated for 4 hrs at 800 C^o. After the powder of BZN was produced, a pellet of BZN was pressed at pressure of 2 MPa, and synthesis at temperature 900 C^o – 1100 C^o for 4 hrs. By this method doped BZN ceramic with the $Bi_{1.5-X}La_XZn_{0.92}Nb_{1.5}O_{6.92}$ empirical formula was produced.

3.2 Structural measurements:

The X-ray diffraction a very important technique used to identify structural properties of the samples. The crystalline nature was identified by XRD technique using Miniflex 600-X-ray diffraction unit that generate X-ray beam at wavelength of 1.5405 A. The X-ray source was fixed at 40 KV to generate X-ray beam from tube of 15 mA current. To get high resolution of the XRD a 0.1 mm slit were used in the XRD system. The X-ray unit is shown in Fig.3.1. We studied the effect of doping ratio on the structure by taking XRD for all samples from X= 0.10 to X= 0.22 at room temperature and lattice parameters were refined by least square method. The temperature effect on the structure of the samples doped with La of X= 0.10 and X= 0.20 was studied in the range from T=298 to T= 470 $^{\circ}K$ by increasing 40 degrees for each trial.

Fig.3.1: The x-ray diffractometer

3.3: Electrical measurements:

The impedance spectroscopy analysis one of the devices that are used to define of the electrical properties of materials. The system measures the impedance, resistance, capacitance, reactance, dielectric constant, and conductance as function of frequency in the range of 10 MHz - 1800 MHz. The impedance spectroscopy analysis was done for RLC circuit which is connected in series and parallel. The values for series and parallel usually are the same. The difference between them, the current is constant and changing in voltage in parallel but, in series the voltage is constant and changing in current. For the purpose of easy measurement, the samples were affected the analyzer by using silver and carbon

pastes. The electrical resistivity of the pyrochlore ceramics was measured using a homemade cryostat that can reach 500 K in air atmosphere. The temperature is manually controlled by using K-type thermocouple and 3 A voltage source. The voltage was supplied to the electrodes from a keithely 235 voltage source and the current was recorded with the help of a keithely 485 Pico ammeter. To get sure about the stability the measurements were repeated at different times and approximately, the same data were produced.

Chapter Four
Results and Discussion

4.1: Doping ratio effect for La-BZN

Figure 4.1 shows an XRD spectra taken for pyrochlore ceramics (BZN) with stoichiometry formula $Bi_{1.5-X}La_XZn_{0.92}Nb_{1.5}O_{6.92}$ that doped with lanthanum of content of X= 0, 0.10, 0.15, 0.20, 0.21 and 0.22. The resulting XRD patterns were first compared to those of the pure BZN. All XRD patterns were analyzed with the help of "TREOR92" software package to reveal the lattice parameter, the plane orientations and volume of unit cell. It was observed that the BZN exhibit cubic lattice. It is important to notice that the intensity of the main peak of the X-ray diffraction patterns increases with increasing doping content. Namely, the main peak exhibit intensity of 467, 585, 774, 3610 and 810 (a.u) for 0.10, 0.15, 0.20, 0.21 and 0.22 La-BZN respectively. The more intensive the X-ray pattern, the better orientation of the planes is the (222) direction. The X-ray diffraction patterns indicate that the $Bi_{1.5-X}La_XZn_{0.92}Nb_{1.5}O_{6.92}$ face centered cubic. The cubic structure includes face centered cubic (FCC), when the miller indices (*h, k, l*) are either all even or all odd, and body centered cubic (BCC), when the sum of miller indices ($h+k+l$) should be even [25]. Since the miller indices for most of the peaks are even and other less intensive all odd [11], so the pyrochlore exhibits (FCC) structure with planes best oriented in the (222) direction.

To understand the reasons buoying beyond this observation, the mechanical properties including the lattice constant, micro strain, dislocation density and degree of orientation are studied and analyzed. The study is carried in accordance with the peak broadening of the (222) plane direction. In accordance with the software results, three solutions are obtained for the lattice parameter however, the selected solution refer to the solution of least error

(less than 0.1 %). The error reduction was actualized by the least square of residual sums and by comparing the difference in the observed and calculated 2θ and restricting to a minimum value.

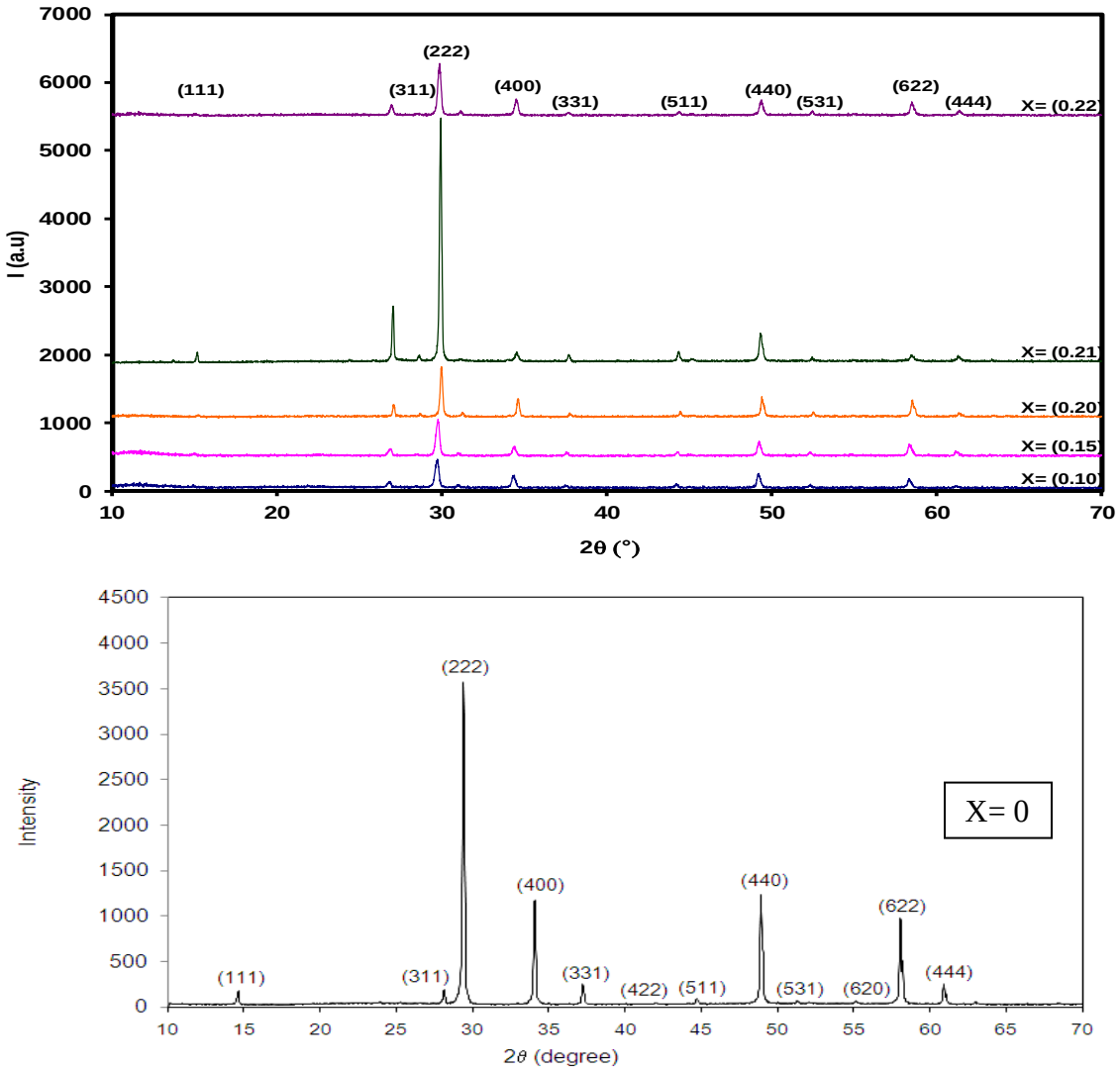

Fig.4.1: The X-ray diffraction patterns of X= 0.10 to X= 0.22 for $Bi_{1.5-X}La_XZn_{0.92}Nb_{1.5}O_{6.92}$ solid solutions at room temperature. (Ref.: Osman, R. A., Maso, N., & West, A. R. (2012). Bismuth Zinc Niobate Pyrochlore, a Relaxor-Like Non-Ferroelectric. *Journal of the American Ceramic Society*, *95*(1), 296-302.)

Table 4.1: 2θ, inter planer space and intensity for maximum peak as a function of La content for the BZN ceramics at room temperature (298 K).

Doping ratio	2θ (°)	Inter plane space d (A)	Intensity I (a.u)
0.10	29.73	3.0029	467
0.15	29.76	2.9999	585
0.20	29.97	2.9794	774
0.21	29.94	2.9823	3610
0.22	29.86	2.9901	810

The maximum peak shifted from 2θ= 29.73 to 2θ=29.97 as doping ratio increase from X= 0.10 to X= 0.20 and it is shifted to 2θ=29.86 at X= 0.22. The inter planer spaces decreased from 3.0029 A to 2.9794 A as doping ratio increases from X= 0.10 to X= 0.20 and increased to 2.9901 at X= 0.22. The intensity increased from 467 a.u to 3610 a.u as doping ratio increase from X= 0.10 to X= 0.21 and decreased to 810 a.u at X= 0.22.

Table 4.2: The mechanical parameters as a function of La content for the BZN ceramics at room temperature (298 K).

Doping ratio	Lattice constant a (A)	Strain $\varepsilon \times 10^{-3}$	Grain size D (nm)	Dislocation density $\delta \times 10^{10}$ (Line/cm^2)
0.10	10.3901	4.27	33.02	18.68
0.15	10.3799	4.27	33.02	18.68
0.20	10.3088	2.61	53.69	7.06
0.21	10.3189	2.45	57.29	6.21
0.22	10.3459	3.60	39.04	13.37

The mechanical properties are also studied as function of the doping ratio. Particularly, the lattice constant, the grain size, the micro strain and the defect density are all calculated from the observed 2θ and the peak broadening at full wave half maximum using the equations $a= d\times(h^2+k^2+l^2)^{1/2}$, $D= (0.94\times\lambda) / (\beta\cos\theta)$, $\varepsilon= (\beta\cos\theta)/(4\times\sin\theta)$ and $\delta= (15\times\varepsilon)/(a\times D)$ respectively. The results are tabulated and plotted in table 4.2 and Fig.4.2. The purpose of the figure is to show the variation in better way. As observed from the presented data, the Lattice constant decreased from 10.3901 (A°) to 10.3088 (A°) as the doping ratio increase from X= 0.10 to X= 0.20. The lattice constant decreased in the single phase pyrochlore so, no new secondary phase appeared from X= 0.10 to X=

0.20 [26]. It is reported that the decrease in the lattice constant for BZN doped by Ni with increasing the content of Ni attributed to the ionic radius of Ni being larger than that of Nb [16]. So, the decrease in the lattice constant as La content increases may be due to the ionic radius of La (1.18 A°) being larger than that of Bi (1.17 A°). The lattice constant increases for X= 0.21 and for X= 0.22 doped samples. This increase may be due to a new minor phase which could have appeared because the lattice constant in the single-phase decreases[15]. La is known to exhibit hexagonal type of structure with lattice parameter of a = 3.772 A, c = 12.144 A, $\alpha = \beta = 90$ and $\gamma = 120$. It is an element of the P63/mmc space group. The properties of this element with ionic radius 1.18 A replaces the vacant sites of Bi. The crystal structure of Bi is monoclinic which refer to the space group C2/m (group number 12). It exhibits lattice parameter of a = 6.674 A, b = 6.117 A and c = 3.304 A. $\alpha = 90 = \gamma$ and $\beta = 120$. Although the solid-state solution is simply actualized by the substitution process. The shape of the unit cell of the two element is very different and create slightly in stable distribution of unit cells.

The BZN is formed from Bi_2O_3-ZnO-Nb_2O_5. The Bi_2O_3 is monoclinic. It is structure is built up of equivalent layers parallel the y-z plane, every second layer consist of Bi atoms. The coordination about Bi is 5 or 6-fold and both arrangements can be described starting from distorted octahedra. The Bi_1 atoms have oxygen nearest neighbors at 5 of the vertices of a distorted octahedron at distances from 2.08-2.63 A and a sixth at 3.25 A of 6 oxygen atoms of distances from 2.14-2.80 A. Three of these are appreciably closer (2.14-2.29 A) then, the other three (2.48-2.8 A). None tetrahedrally bonded elements and binary [27]. On the other hand, Li_2O_3 has seven-fold coordinated with four short La-O bonds (2.30 A) and three longer bonds (2.70 A), it has hexagonal structure. The oxygen ions are in octahedral

shape around the metal atom and there is one oxygen ion above one of the octahedral faces. It converts to cubic at high temperature and become surrounding 6 coordinate group of O^{-2} ions.

Since the amount of La is increasing the number of bonds that are not regularly distributed upon replacement of Bi with La increases. It seems that as shown in table 4.1 when the La content reaches 0.20, the number of irregular bonds become significant to create extra strain on the cells and thus leads to the decrease in the lattice constant such instability in the structure motivate the formation of some minor phases as seen from the EDS tests.

Some minor phase may be return to $BiLaO_3$, $LaNbO_3$ and ZnO. To make sure about these phases in the La-BZN, the scanning electron microscope (SEM), and energy dispersion X-ray analysis (EDS) measurement performed. The SEM image appeared at X= 0.21 all La solubility as shown in Fig.4.3 (a) and at X= 0.22 sample. The solubility limit of the La doped pyrochlore and the appeared new grains at this sample are shown in Fig.4.3 (b). The EDS quatative and quatitove analysis show that the minor phase related to the $LaNbO_3$ phase, the pyrochlore phase and ZnO phase as shown in Fig.4.3 (c, d and e) [11]. The strain and grain size are calculated from Scherer equation [28]. The strain was decreased from $(4.27 \text{ to } 2.45)\times 10^{-3}$ as doping ratio increases from X= 0.10 to X= 0.21 may be due to the variation in the imperfection in the crystalline lattice and dislocation density. The large lattice mismatch of the between the solved elements and the unbonded as well as vacant oxygen sites disturb the balancing forces at the lattice points and that in turn leads to the existing micro strain [29], and then increased to 3.60×10^{-3} at 0.22 may be due to increased in lattice constant and new phase appeared in this sample. A.F. Qasrawi et al. [3] studied

doping BZN by Ta, as reported the grain size decrease as Ta increase, due to the internal energy re-stabilization, in which the increase in grain sizes occurs when recovery and recrystallization are complete and reducing the total area of grain boundary is the only possible way for reducing in the internal energy. The grain size was increased from 33.02 to 57.26 (nm) with doping ratio increases from X= 0.10 to X= 0.21, may be due to reducing the total area of grain boundary by recovery and recrystallization are complete and further reduction in the internal energy, and then decrease at X= 0.22 to 39.04 (nm), may be attributed to the internal energy re-stabilization [13]. The dislocation density decreased from (18.68 to 6.21) $\times 10^{10}$ (line/cm^2) with increase in doping ratio from 0.10 to 0.21 may be due to the decrease in the strain and then increased to 13.37×10^{10} (line/cm^2) at X= 0.22. The latter is assigned to re-increase in the strain that arises from the instable bond of La-O. Fig.4.3 show the scanning electron microscope images for a balk scattered image for the pyrochlore ceramics doped with 0.21 and 0.22 La. While the image of (a) which refer to 0.21 doping content have single type of grains, the second content islands of different type. We note these islands with number 1, 2 and 3. The EDS analysis, show the presence of the BZN at point 2. The point 1 refer to $LaNbO_3$ and the point 3 refer to ZnO phase.

It is also noticeable that the grain size of BZN is about 1 μm. This result is in contradiction with these XRD. The different between the two techniques lay in the fact that the Scherer equation can only read grains of size less than 0.2 μm. As they the data which are recorded by XRD technique must refer to crystallites of nano sizes that accumulate to form grains of micro size.

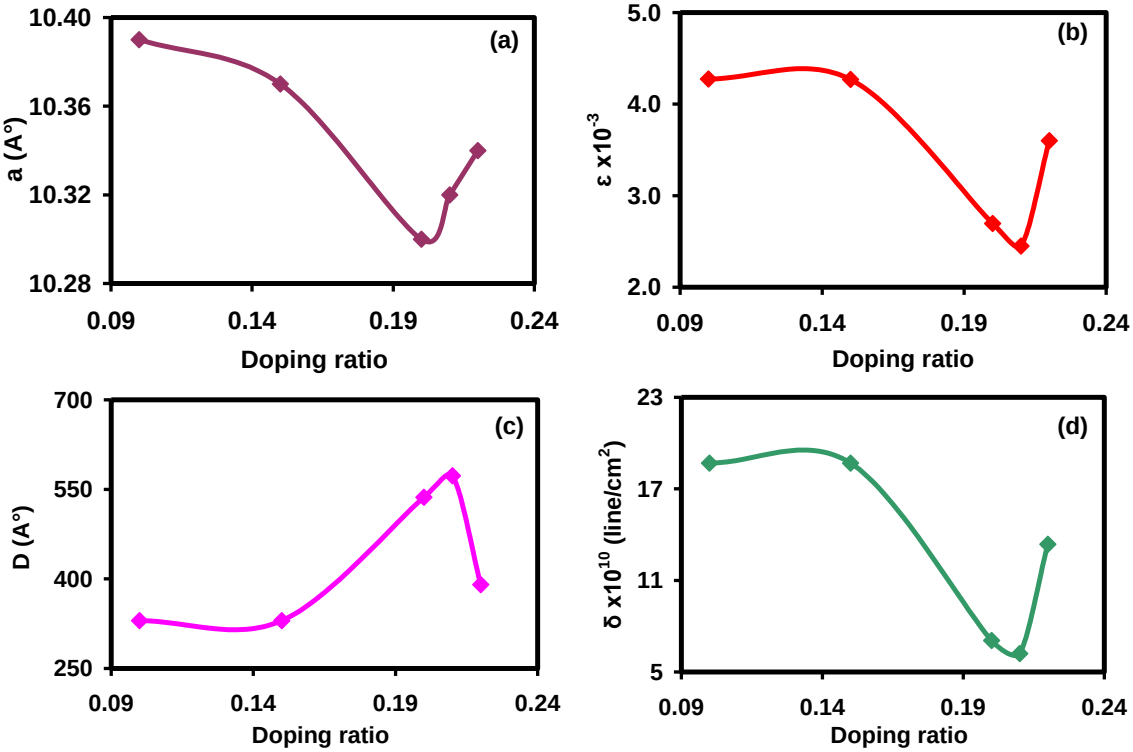

Fig 4.2: (a) Lattice constant (b) Strain (c) Grain size (d) Dislocation density of La-BZN as a function of doping ratio.

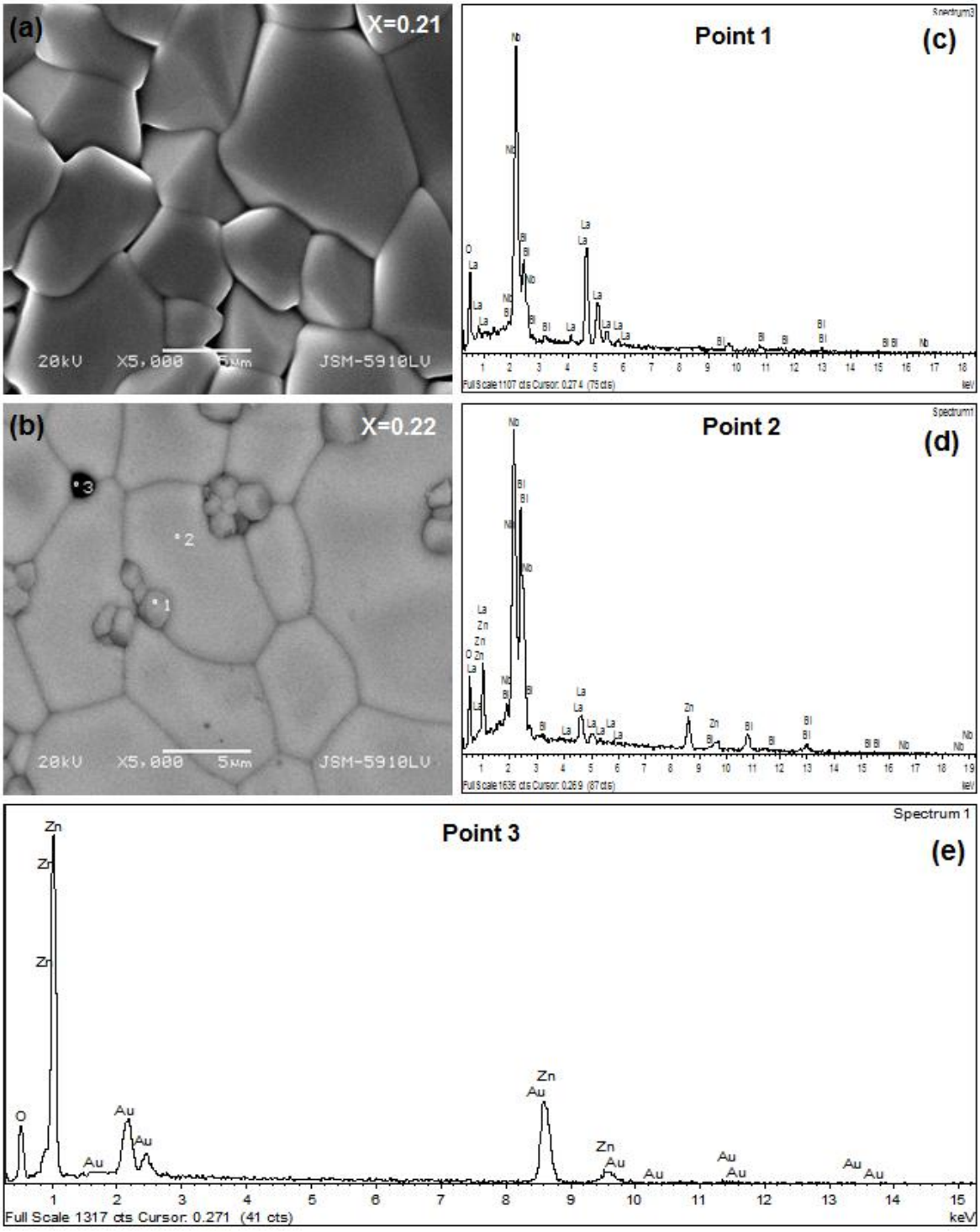

Fig.4.3: The SEM images for (a) the $Bi_{1.29}La_{0.21}Zn_{0.92}Nb_{1.5}O_{6.92}$ (b) $Bi_{1.28}La_{0.22}Zn_{0.92}Nb_{1.5}O_{6.92}$ solid solution and EDS analysis for (c) point 1, (d) point 2 and (e) point 3 which are presented in image (b).

4.2: The thermal properties of La-BZN

The pyrochlore ceramics $Bi_{1.5-X}La_XZn_{0.92}Nb_{1.5}O_{6.92}$ with X= 0.10 and X= 0.20, were studied with temperature from 298 $^{\circ}$K to 470 $^{\circ}$K. The deformation is any change in the size or shape of the object due to an applied force or change into the temperature, the difference between them is how the energy transferred. In the deformation output from an applied force, the energy transferred through the work, but the energy transferred through heat if the deformation caused by the change in temperature, which can determine several factors such as lattice constant, strain, grain boundaries and dislocation density.

4.2.1: Temperature dependent XRD analysis for $Bi_{1.4}La_{0.1}Zn_{0.92}Nb_{1.5}O_{6.92}$

As the temperature increase from 298 $^{\circ}$K to 470 $^{\circ}$K, the maximum peak also shifts from 29.76° to 29.45° as shown in (Fig4.4). Shifting position due to as temperature increases, the kinetic energy increase and more energy should be available for the atoms to move, so the energy will be not stabilization and the peaks shifts [30]. The peaks inside the circle in Fig. 4.4 corresponds to the base of the steel on which the sample is placed.

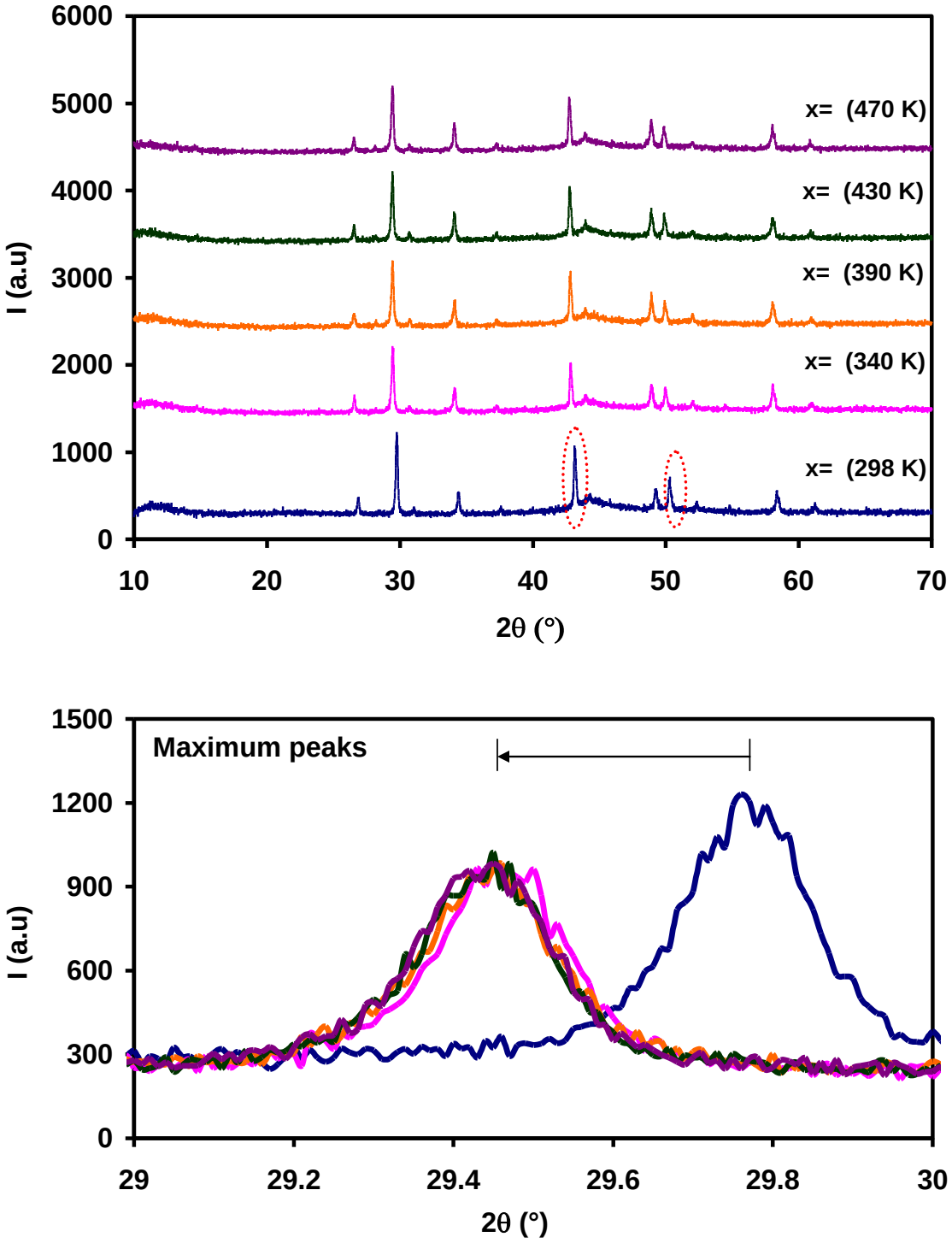

Fig. 4.4: X-ray diffraction patterns for $Bi_{1.5-X}La_XZn_{0.92}Nb_{1.5}O_{6.92}$ with X= 0.10 as a function of temperature.

Table 4.3: The mechanical parameters for 0.10-La-BZN as function of temperature.

Temperature T (°K)	Lattice constant a (A°)	Strain $\varepsilon \times 10^{-3}$	Grain size D (nm)	Dislocation density $\delta \times 10^{10}$(Line/cm^2)
298	10.3901	4.27	33.02	18.68
350	10.4867	3.15	45.16	9.99
390	10.4832	3.15	45.16	9.99
430	10.4867	2.65	53.62	7.08
470	10.4867	3.32	42.90	11.07

The mechanical properties were studied with temperature from 298(°K) to 470(°K) as shown in Fig.4.5. The lattice constant increased from 10.3901 A to 10.4867 with temperature increasing from 298 K to 350 K, at 390 K lattice constant decreased to 10.4832 A, re-increased to 10.4867 A at 430 K and remain constant until they reached to 470 K. The strain decreased from 4.27×10^{-3} at 298 K to 2.65×10^{-3} at 430 K and increased at 470 K to 3.32×10^{-3}. The grain size increased from 33.02 nm to 53.62 nm with temperature increasing from 298 K to 430 K and decreased to 42.90 nm at 470 K. The behavior of dislocation density and strain is same, were dislocation density decreased from 18.68×10^{10} line/cm^2 at 298 K to 7.08×10^{10} line/cm^2 at 430 K and increased to 11.07×10^{10} line/cm^2 at 470 K. From Fig.4.8 (a), we can see the change in lattice constant (Δa) with temperature, when Δa decreased as temperature increase, the strain $\varepsilon = \Delta a/a$ will be decrease. The

reason is possible to reducing in the internal energy and the energy is more stable and the decrease in dislocation density related to decrease in the strain. But, the increase in grain size attributed to reducing in the internal energy and the energy is more stable [31]. At 470 K, strain and dislocation density are increased due to the energy in not stable so, the grain size decreased to re-stabilization of energy.

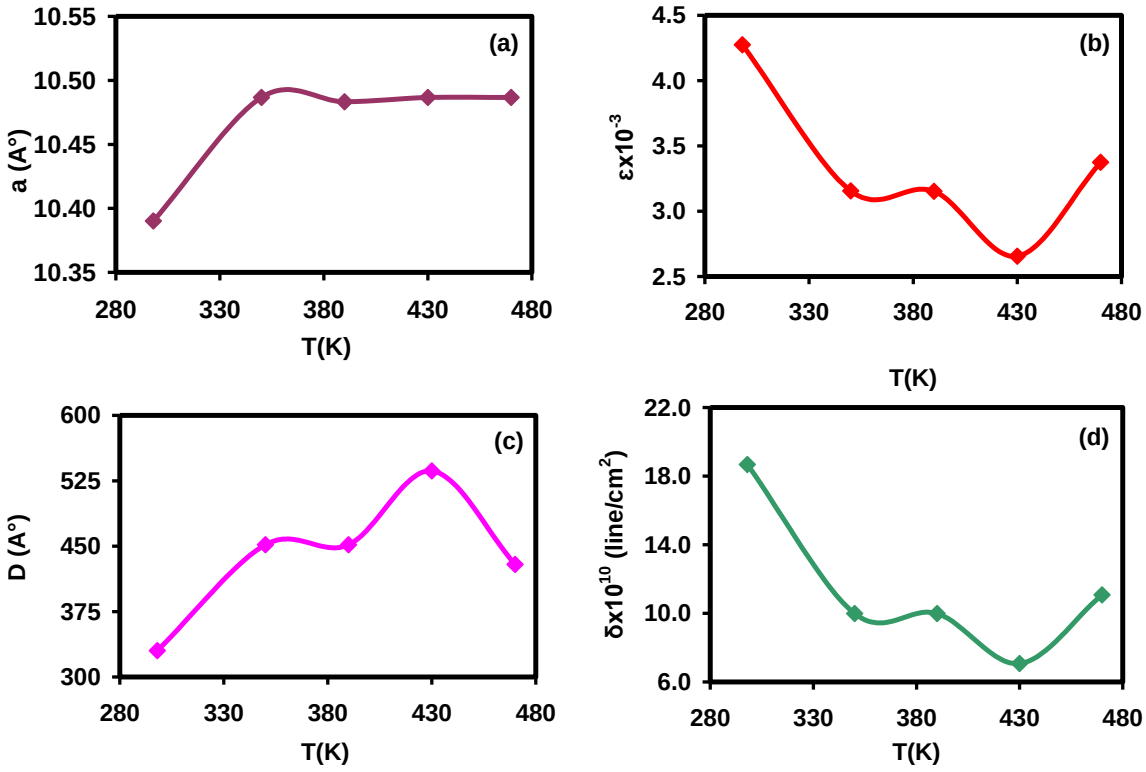

Fig 4.5: (a) Lattice constant (b) Strain (c) Grain size (d) Dislocation density of La-BZN as a function of temperature for X= 0.10.

4.2.2: Temperature dependent XRD analysis for $Bi_{1.3}La_{0.2}Zn_{0.92}Nb_{1.5}O_{6.92}$

By increasing the temperature, the maximum peak also shifting corresponding 2θ from 29.71° to 29.705° and the intensity increased in general as shown in (Fig4.6). The shift in the peaks assigned to change in internal energy with temperature as explained previously. But, the increase in the intensity attributed to high preferential oriented [32] and crystalline quality of the sample [33]. The peaks inside the circle in Fig. 4.6 correspond to the base of the steel on which the sample is placed.

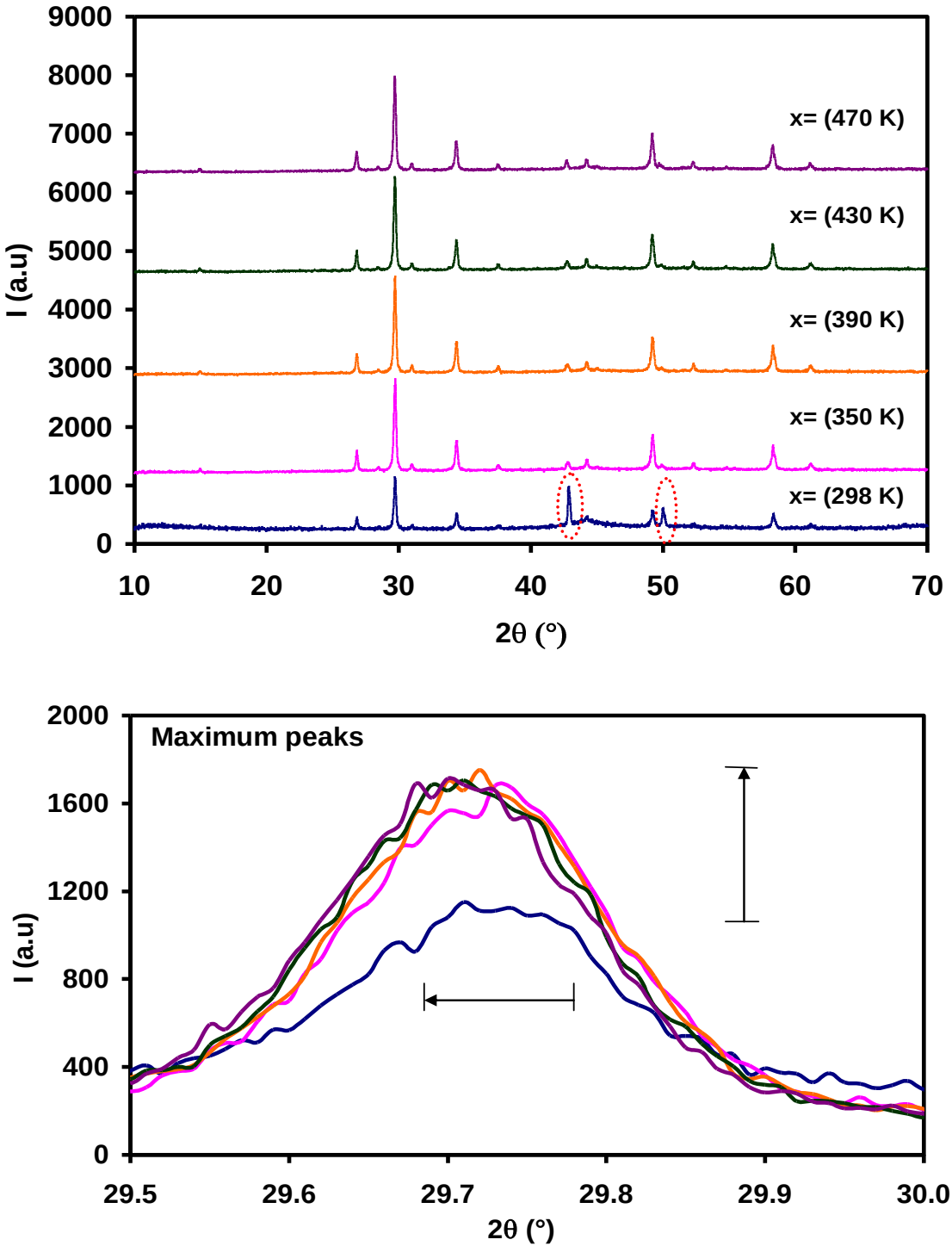

Fig.4.6: X-ray diffraction patterns for $Bi_{1.5-x}La_xZn_{0.92}Nb_{1.5}O_{6.92}$ with X= 0.20 as a function of temperature.

Table 4.4: The mechanical parameters for 0.20-La-BZN as function of temperature.

Temperature T (°K)	Lattice constant a (A°)	Strain $\varepsilon \times 10^{-3}$	Grain size D (nm)	Dislocation density $\delta \times 10^{10}$ (Line/cm^2)
298	10.3088	2.61	53.69	7.06
350	10.3850	3.12	45.20	9.97
390	10.3918	3.28	42.93	11.05
430	10.3953	3.29	42.92	11.05
470	10.3987	3.12	45.20	9.98

The mechanical properties were studied for 0.20 (La-BZN) with temperature from 298 K to 470 K as shown in Fig.4.7. The lattice constant increased from 10.3088 A° to 10.3987 A° with temperature increases from 298 K to 470. The strain increase from 2.60×10^{-3} to 3.29×10^{-3} with temperature increases from 298 K to 430 K, and then decreased to 3.12×10^{-3} at 470 K. The grain size decreased from 53.69 nm to 42.92 nm with temperature increases from 298 K to 430 K, and then increase to 45.20 nm at 470 K. The dislocation density increased from (7.06 to 11.05)$\times10^{10}$ line/cm^2 with temperature increases from 298 K to 430 K, and then decreased to 9.98×10^{10} line/cm^2 at 470 K. The change in the lattice constant (Δa) increased as temperature increases from 298 K to 430 (°K) as shown in Fig.4.8 (b) and the strain increased assigned to change in the internal energy and not stabilization. The change in the dislocation density attributed to change in the strain and

the decrease in the grain sizes assigned to energy re-stabilization as mentioned earlier. At 470 K the energy is more stabilization because the strain and dislocation density were decreased but, grain size increased.

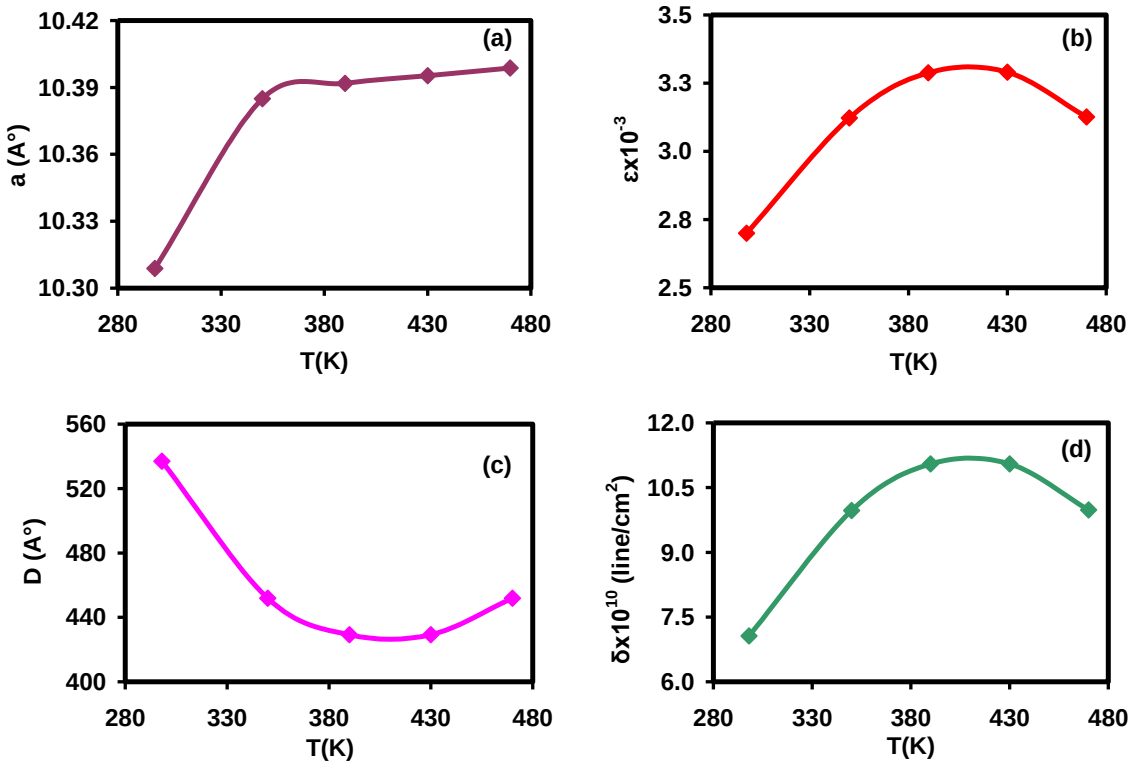

Fig 4.7: (a) Lattice constant (b) Strain (c) Grain size (d) Dislocation density of La-BZN as a function of temperature for X=0.20.

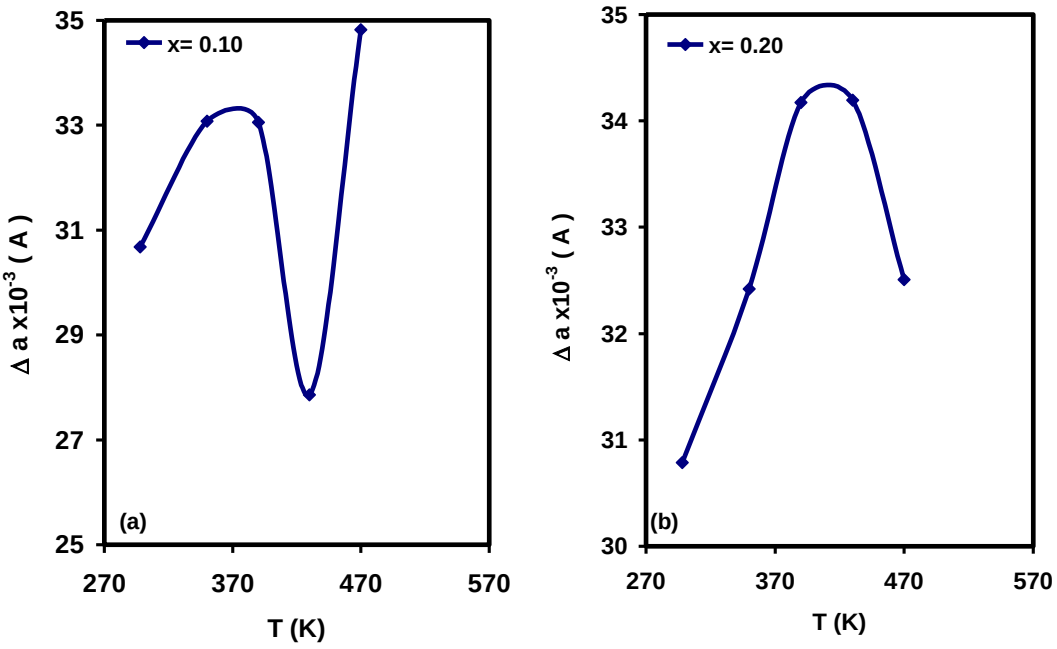

Fig. 4.8: The change in lattice constant (a): X= 0.10 of La doped BZN (b): X= 0.20 of La-BZN as a function of temperature.

4.2.3: Comparison for heating-cooling cycles of X= 0.10 and X= 0.20 La-BZN

Table 4.5: The mechanical parameters for X= 0.10-La-BZN before and after heating.

	Lattice constant a (A)	Strain $\varepsilon \times 10^{-3}$	Grain size D (nm)	Dislocation density $\delta \times 10^{10}$(Line/cm^2)
Before heating	10.3901	4.27	33.02	18.68
Target 470 (°K)	10.4867	3.32	42.89	11.07
After heating	10.3901	4.11	34.34	17.27

Table 4.6: The mechanical parameters for X= 0.20-La-BZN before and after heating.

	Lattice constant a (A)	Strain $\varepsilon \times 10^{-3}$	Grain size D (nm)	Dislocation density $\delta \times 10^{10}$ (Line/cm^2)
Before heating	10.3088	2.61	53.69	7.06
Target 470 (°K)	10.3987	3.126	45.18	9.98
After heating	10.3071	2.608	53.69	7.06

The mechanical parameters, strain and dislocation density for X= 0.10 were decreased after heating but, the grain size increased after heating we can see from table 4.4. As doping ratio increased to X= 0.20, mechanical parameters are the same before and after heating we can see from table 4.5. The decrease in the strain and dislocation density for X=0.10 after heating related to reducing in the internal energy and the energy more stable so, the grain size increased after heating for this sample.

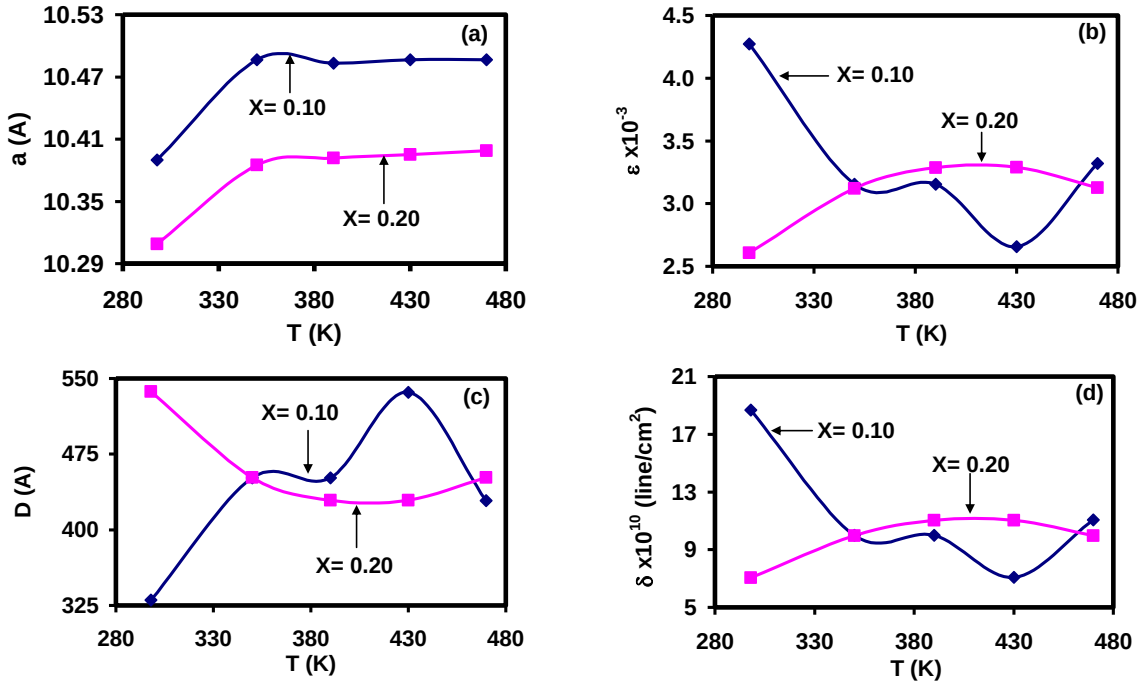

Fig 4.9: (a) Lattice constant (b) strain (c) g (d) dislocation density of La doped BZN as a function of temperature for X= 0.10 and X= 0.20

4.3: Impedance spectroscopy of La doped BZN:

The electrical properties of La-BZN as function of doping ratio were studied in the range of frequency 10 MHz to 1800 MHz, but we take the range of 100 MHz to 1100 MHz because after 1100 MHz appeared oscillation and continued to 1800 MHz Lead to change into mathematical calculations and become incorrect. The measured capacitance, resistance and impedance spectra are displayed in Fig.4.10 (a), (b) and (c) respectively. As seen from Fig.4.10 (a), the capacitance increased as doping ratio increases from 13.5 pFs at X= 0.10 to 20.6 pF at X= 0.22 samples is due to the increase in dielectric constant. Since the dielectric constant represent the degree of electrical polarization, then the increase in the dielectric constant with increasing atomic content in this frequency range should be assigned to the ability of La^{+3} to onent better than the Bi^{+3} ion. The Bi_2 atom has irregular octahedral arrangement of 6 atoms with three short Bi-O bonds while La_2 have 7-fold coordinated atoms with four short La-O bonds. The capacitance is constant with frequency of 100 MHz to 1100 MHz for all samples as shown in Fig.4.10 (a). Oscillations were observed in the frequency range 1100_1800 MHz. As a result, it can be used as practical applications of microwaves. The resistance which is shown in Fig.4.10 (b) decreased with increasing in frequency of 100 MHz to 1100 MHz. The resistance inversely depends on the collision time ($\sigma = n\ e^2\ \tau\ /\ m$), where m and e are mass and charge on the electron respectively, n: free electron density and τ: relaxation time of the free electrons. The collision time increase because of the inability of dipole to oscillate with the externally applied field. As a result, electrons are set free and more random motion taken place leading to the longer collision time value and lower resistance [35]. The change in

resistance with doping ratio is very small and not systematic. The impedance was decreased with frequency increasing for all ratios of 100 MHz to 1100 MHz as shown in Fig.4.10 (c). The behavior of the impedance as like behavior the resistance, that means all current had become in the resistance, so the capacitance is constant with frequency. The decrease in impedance is guided by resistance as mentioned earlier. The admittance was increased with frequency increasing of 100 MHz to 1100 MHz for all samples, due to the same reasons. The admittance with doping ratio decreased at X= 0.15, at X= 0.20 increased, re-decreased at X= 0.21 and re-increased at X= 0.22 samples, the behavior is not systematic as shown in Fig.4.11 (a). The conductance increased as frequency increased from 100 MHz to 1100 MHz, may be due to the increase in admittance, but the conductivity is constant with doping ratio as shown in Fig.4.11 (b). The dielectric constant spectra which shown as in Fig.4.12 confirm the behavior of capacitance and is assigned for the same reasons.

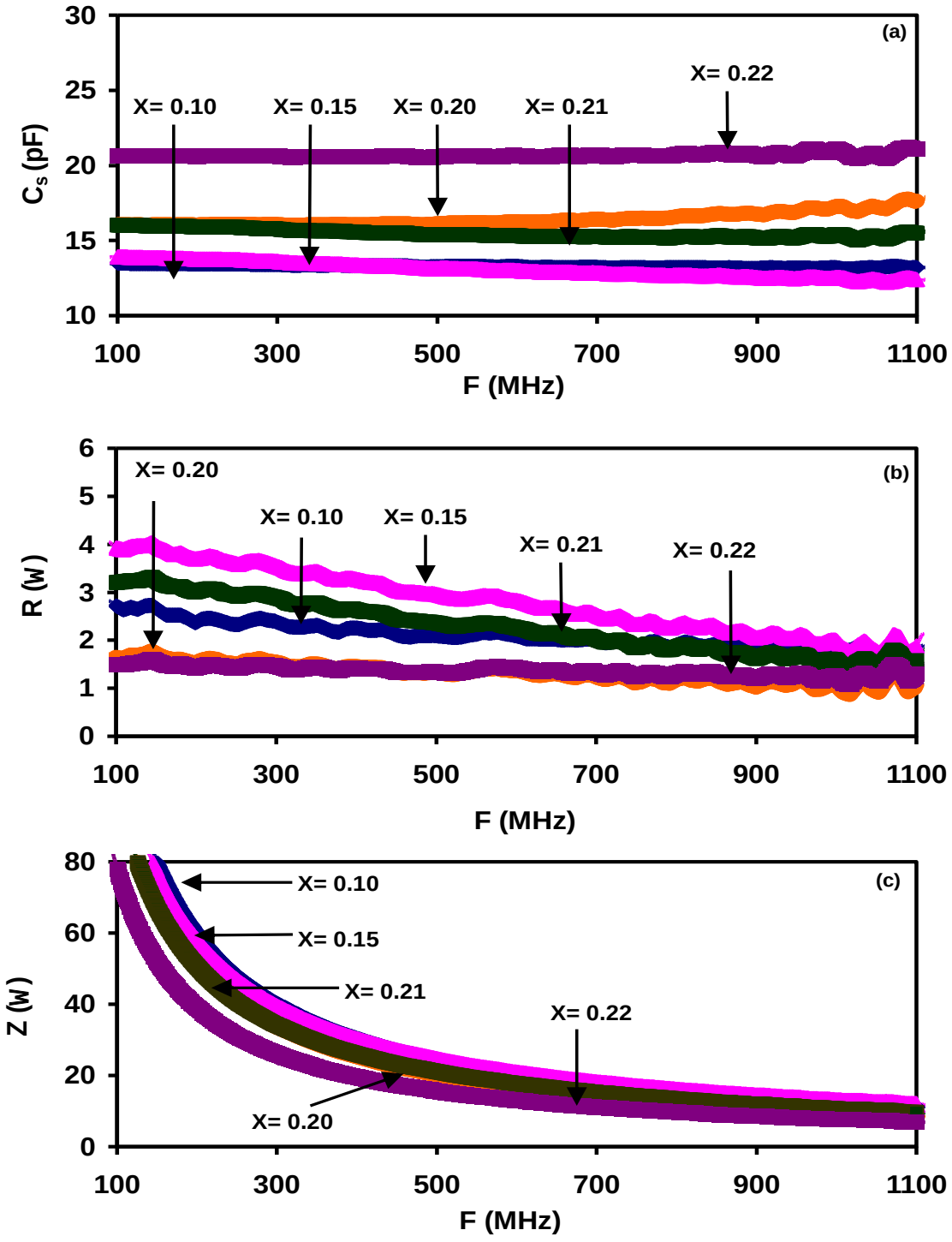

Fig.4.10: (a) Capacitance (b) Resistance (c) Impedance of La-BZN as a function of frequency

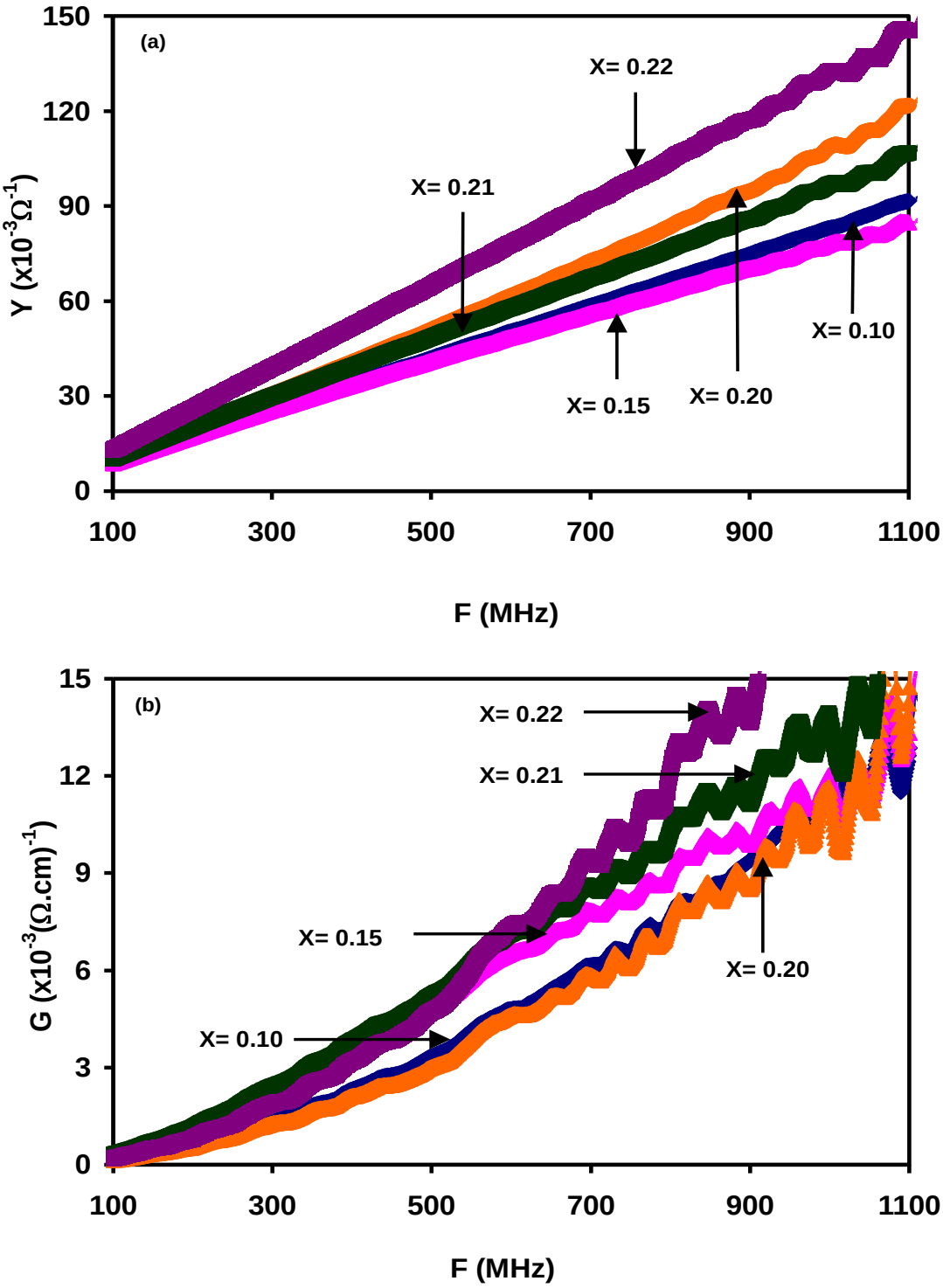

Fig.4.11: (a) Admittance (b) Conductance of La-BZN as a function of frequency

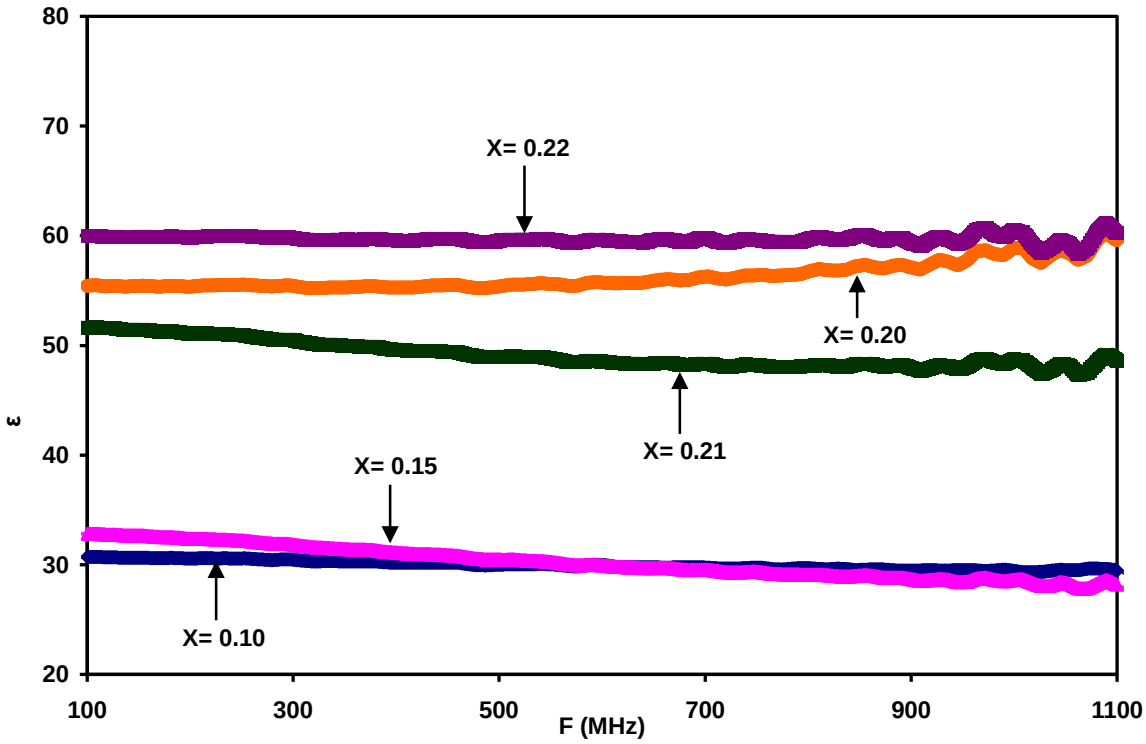

Fig.4.12: Dielectric constant of La-BZN as a function of frequency

4.4 Electrical properties:

To explore the effect of the La doping on the electrical performance of the BZN, the temperature dependent electrical conductivity was measured for all the samples. The electrical conductivity remains constant with temperature for 0.10, 0.21 and 0.22 samples below 483 K as shown in Fig. 4.13. Above this temperature, for these samples, the electrical conductivity exhibit sharply from low conductivity to high conductivity values. For 0.15 and 0.20 samples, the electrical conductivity exhibit sharply above 473 K and 433 K respectively from low conductivity to high conductivity values. The plot of the ln (σ) as function of temperature as shown in Fig. 4.13 revealed the activation energies for La-BZN as shown in table 4.6.

Table 4.7: The activation energy of La-BZN from X= 0.10 to X= 0.22

La content	0.10	0.15	0.20	0.21	0.22
Ea (eV)	1.75	1.24	1.64	1.72	1.74

The activation energy for 0.10, 0.21 and 0.22 is greater than of half of energy band gap 3.30 eV, but for 0.15 and 0.20, the activation energy is less than of the half energy band gap. When the activation energy is greater than of half of the energy band gap, the type of conduction is intrinsic [12]. The activation energy as per the transition-state theory, is the difference in energy content between an activated or transition-state configuration to that of the corresponding initial configuration [34]. The sharp increase in electrical conductivity at a particular temperature, can be assigned to accelerating electron motion. Electrons in the valance band gain enough thermal energy to reach the conduction band [29].

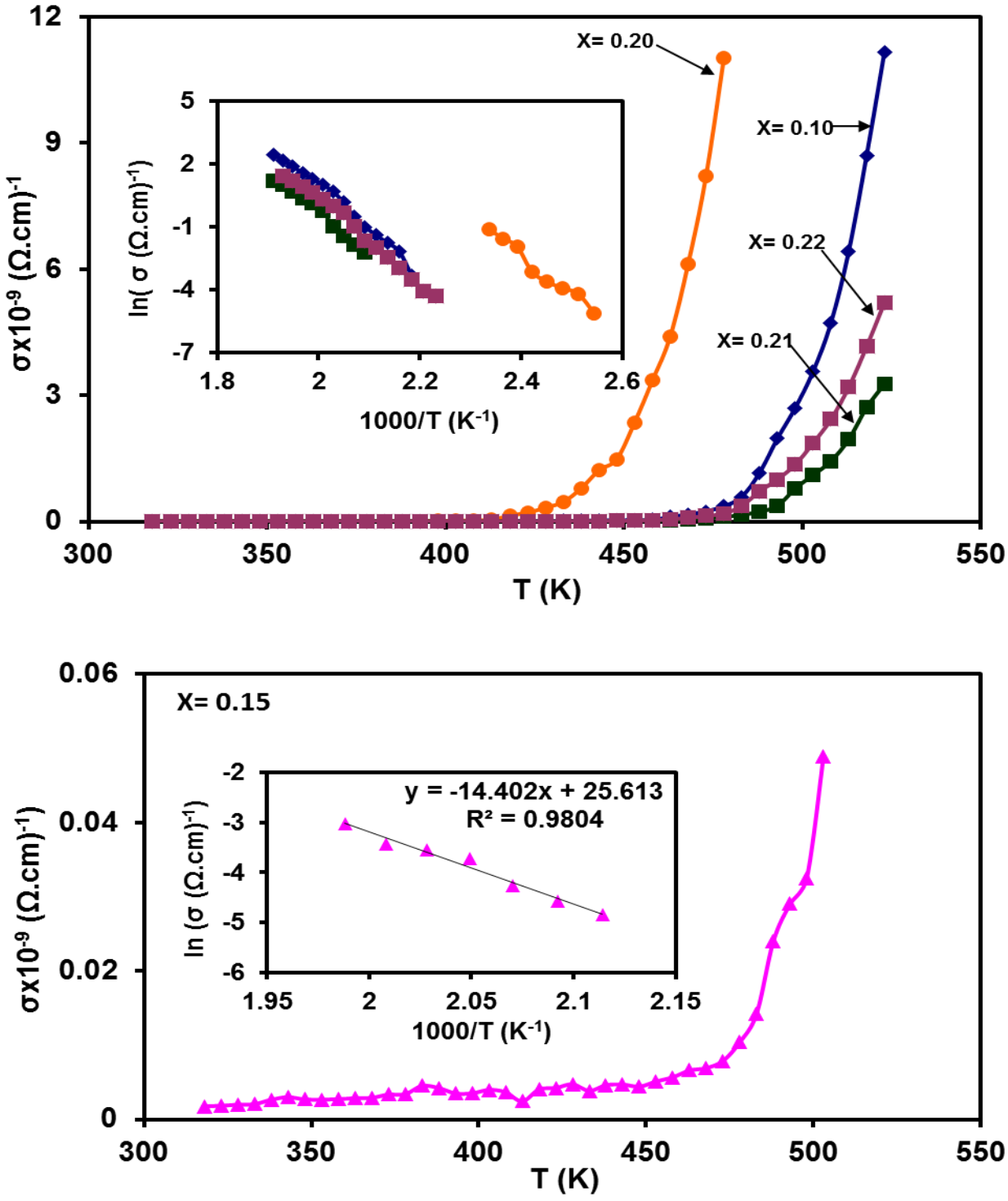

Fig.4.13: Variation of electrical conductivity of the La-BZN with temperature. The inset shows the ln (σ)-T^{-1} dependence.

Conclusions:

In this thesis, we have discussed the problem of enhancing the electrical and dielectric properties of the $Bi_{1.5}Zn_{0.92}Nb_{1.5}O_{6.92}$ through doping it with rare earth element. The doping was varied in the rate of 0.10-0.22 as an atomic content which replaces the Bi atoms in the structure. The doping effects on the structural properties was studied by the X-ray diffraction technique. Analysis of the results that analyzed from this method arrived at a solubility limit of La content of 0.20 within the range of solubility, the lattice constant and grain size appeared as a systematically behaving parameter that control all the structure. It was observed that when the solubility limit is exceeded, then minor phases of $LaBiO_3$, the pyrochlore and ZnO appeared. The presence of the minor phase in the structure of BZN increased the disorder in the system and strongly affect it is electrical performance.

In as a temperature to enhance it is crystallinity and induce the solubility, the doped pyrochlore ceramics were subjected to heat treatment in the range of 300-470 K. The temperature dependent X-ray analysis have shown that for low doping content of La, the lattice constant increased permanently while heaving doped BZN show no response to temperature effect. All physical parameters are accordingly attenuated.

On the other hand, the electrical measurements have shown then a significant enhancement in the dielectric constant was achieved by the doping process, this enhancement is associated with low value of nonsystematic resistance frequency response indicating that the impedance and all other electrical parameters are guided by the free electrons in the samples that in turn result in decreasing resistance.

The electrical conductivity measurements in the temperature range of 318-523 K have shown that the doping agent of less effected on the electrical behavior the impurity level is very deep and oscillates near 1.8 eV. The doping of La into BZN is still need further study that concentrate on lowering that electrical resistance which should enhance the impedance behavior of the pyrochlore prior to technological applications.

Referemces:

[1] Huiling, D., & Xi, Y. (2002). Dielectric relaxation characteristics of bismuth zinc niobate pyrochlores containing titanium. *Physica B: Condensed Matter, 324(1), 121-126.*

[2] RC Ewing, WJ Weber, J Lian. (2004). Nuclear waste disposal-pyrochlore (A2B2O7): Nuclear waste form for the immobilization of plutonium and "minor" actinides. *Journal of Applied Physics, 95(11).*

[3] Qasrawi, A. F., & Mergen, A. (2012). Structural, electrical and dielectric properties of Bi 1.5 Zn 0.92 Nb 1.5− x Ta x O 6.92 pyrochlore ceramics. *Ceramics International, 38(1), 581-587.*

[4] Zhang, X., Ren, W., Shi, P., Tian, A., Xin, H., Chen, X., ... & Yao, X. (2010). Influence of substrate temperature on structures and dielectric properties of pyrochlore Bi 1.5 Zn 1.0 Nb 1.5 O 7 thin films prepared by pulsed laser deposition. *Applied Surface Science, 256(22), 6607-6611.*

[5] Qasrawi, A. F., Kmail, B. H., Nazzal, E. M., & Mergen, A. (2013). Investigation of the physical properties of Bi1. 5-xCdxZn0. 92Nb1. 5O6. 92-x/2 pyrochlore ceramics. *Journal of Electroceramics, 31(1-2), 61-66.*

[6] Qasrawi, A. F., Kmail, B. H., & Mergen, A. (2012). Synthesis and characterization of Bi 1.5 Zn 0.92 Nb 1.5− x Sn x O 6.92− x/2 pyrochlore ceramics. *Ceramics International, 38(5), 4181-4187.*

[7] Al Garni, S. E., Qasrawi, A. F., & Mergen, A. (2016). Physical properties of the Bi 1.5 Zn 0.92− 2x HfxNb 1.5 O 6.92 solid solutions. *Ceramics International, 42(2), 3372-3379.*

[8] Qasrawi, A. F., & Mergen, A. (2013). Effect of yttrium solubility on the structural and optical properties of Bi 1.5− x Y x Zn 0.92 Nb 1.5 O 6.92 pyrochlore ceramics. *Ceramics International, 39(8), 8687-8692.*

[9] Choi, Y., Kim, I. D., Tuller, H. L., & Akinwande, A. I. (2005). Low-voltage organic transistors and depletion-load inverters with high-K pyrochlore BZN gate dielectric on polymer substrate. *IEEE Transactions on Electron Devices, 52(12), 2819-2824.*

[10] Qasrawi, A. F., Kmail, R. R., Mergen, A., & Genc, S. (2016). Mechanical and electrical properties of Bi1. 5-xLaxZn0. 92Nb1. 5O6. 92 pyrochlore ceramics. *Journal of Electroceramics, 37(1-4), 8-14.*

[11] Qasrawi, A. F., Muis, K. O. A., Rob, O. H. A. A., & Mergen, A. (2014). Electrical characterization of Bi 1.50-x Y x Zn 0.92 Nb 1.5 O 6.92 varactors. *Functional Materials Letters, 7(04).*

[12] Qasrawi, A. F., Bzour, F. M., Nazzal, E. O., & Mergen, A. (2014). Electrical conductivity and capacitance spectra of Bi 1.37 Sm 0.13 Zn 0.92 Nb 1.50 O 6.92 pyrochlore ceramic in the range of 0–3 GHz. *Functional Materials Letters, 7(02).*

[13] Tianxiu, S., Shihua, D., Qian, Z., & Zhuowei, Z. (2013). The effect of MgO on the structure and dielectric properties of α-BZN ceramics. *Ferroelectrics, 451(1), 62-67.*

[14] Mergen, A., Özyoldaş, O., & Küçük, İ. (2012). Production and properties of In and Ir doped Bi 1.5 Zn 0.92 Nb 1.5 O 6.92 pyrochlores. *Journal of the European Ceramic Society, 32(9), 2019-2023.*

[15] Qasrawi, A. F., Nazzal, E. M., & Mergen, A. (2012). Structural, optical, electrical and dielectric properties of Bi1· 5Zn0· 92Nb1· 5− xNixO6· 92− 3x/2 solid solution. *Advances in Applied Ceramics, 111(3), 165-170.*

[16] Brinker, C. J., & Scherer, G. W. (2013). *Sol-gel science: the physics and chemistry of sol-gel processing*. Academic press.

[17] Heimann, R. B. (2010). *Classic and advanced ceramics: from fundamentals to applications*. John Wiley & Sons.

[18] Whittig, L. D., & Allardice, W. R. (1986). X-ray diffraction techniques. *Methods of Soil Analysis: Part 1—Physical and Mineralogical Methods*, (methodsofsoilan1), 331-362.

[19] Spence, J. C. (2006). The Way Forward for Electron Crystallography. In *Electron Crystallography*, 31-42. Springer, Dordrecht.

[20] Patterson, A. L. (1939). The Scherrer formula for X-ray particle size determination. *Physical review, 56(10), 978.*

[21] Bindu, P., & Thomas, S. (2014). Estimation of lattice strain in ZnO nanoparticles: X-ray peak profile analysis. *Journal of Theoretical and Applied Physics*, *8*(4), 123-134.

[22] Al Garni, S. E., & Qasrawi, A. F. (2017). Impedance Spectroscopic Analysis of the InSe/ZnSe/InSe Interface. *IEEE Transactions on Electron Devices, 64(1), 244-249*.

[23] Bakshi, U. A., & Bakshi, A. V. (2009). *Network analysis*. Technical Publications.

[24] AILLERIE, M. (2012). Experimental Measurement of Electric Conductivity and Activation Energy in Congruent Lithium Niobate Crystal.

[25] Birkholz, M. (2006). *Thin film analysis by X-ray scattering*. John Wiley & Sons, 1-40.

[26] Mergen, A., Özyoldaş, O., & Küçük, İ. (2012). Production and properties of In and Ir doped Bi 1.5 Zn 0.92 Nb 1.5 O 6.92 pyrochlores. *Journal of the European Ceramic Society, 32(9), 2019-2023.*

[27] Douglas, J. E. (2016). Biphasic thermoelectric materials derived from the half-Heusler/full-Heusler system Ti–Ni–Sn (Doctoral dissertation, University of California, Santa Barbara).

[28] Piumetti, M., Bensaid, S., Russo, N., & Fino, D. (2015). Nanostructured ceria-based catalysts for soot combustion: investigations on the surface sensitivity. *Applied Catalysis B: Environmental, 165, 742-751.*

[29] Qasrawi, A. F., Kmail, R. R., Mergen, A., & Genc, S. (2016). Mechanical and electrical properties of Bi1. 5-xLaxZn0. 92Nb1. 5O6. 92 pyrochlore ceramics. *Journal of Electroceramics, 37(1-4), 8-14.*

[30] Mathew, J. P., Varghese, G., & Mathew, J. (2012). Effect of post-thermal annealing on the structural and optical properties of ZnO thin films prepared from a polymer precursor. *Chinese Physics B, 21(7).*

[31] Mathew, J. P., Varghese, G., & Mathew, J. (2015). Effect of Annealing on the Optical Properties of Transition Metal Doped ZnO Thin Films. In *IOP Conference Series: Materials Science and Engineering, 73(1),* IOP Publishing.

[32] Yadav, A. B., Periasamy, C., & Jit, S. (2015). Study of post annealing effects on structural and optical properties of sol-gel derived ZnO thin films grown on n-Si substrate. In *IOP Conference Series: Materials Science and Engineering, 73(1),* IOP Publishing.

[33] Jian-Ping, X., Shao-Bo, S., Lan, L., Xiao-Song, Z., Ya-Xin, W., & Xi-Ming, C. (2010). Effects of annealing temperature on structural and optical properties of ZnO thin films. *Chinese Physics Letters*, *27*(4), 047803.

[34] Sudha, L. K., Sukumar, R., & Uma Rao, K. (2014). Evaluation of activation energy (Ea) profiles of nanostructured alumina polycarbonate composite insulation materials. *International Journal of Materials. Mechanics and Manufacturing*, *2*(1), 96-100.

[35] Dr. J. P. Goel, D. C. Upadhyay, Er. Meera Goyal. (2016). PHYSICS: Electric conduction and ohms law. Chapter: 5, P: 209-211

Conferences

- Qotiabah A. A. Alkarem, Adli A. Saleh. Hazem. Khanfar, A. F.Qasrawi (poster). Mechanical properties of Terbium doped Nd2Sn2O7, Fifth Palestinian Conference on Modern Trends in Mathematics and Physics, Arab American University-Jenin.

- Qotiabah A. A. Alkarem, Adli A. Saleh. Hazem. Khanfar, A. F.Qasrawi (Poster). Mechanical properties of Lanthanum doped BZN. Second Palestinian International Conference on Material Science and Nanotechnology, An-Najah National University- Nablus.

طيف الممناعة والخواص البنوية والاعتماد على درجة الحرارة للسيراميك المطعم (La-BZN)

اعداد

قتيبة عبد الهادي عبد القادر الكرم

اشراف

دكتور عدلي صالح

والمشرف

دكتور حازم خنفر

الملخص

نظرا لشهرة تطبيقاتها كمادة ذات عازلية مرتفعة، في هذه الرسالة سنستكشف بعض الخصائص المميزة للسيراميك البزموث زنك نيوبيوم اوكساید المطعم بعنصر اللانثانوم $Bi_{1.5-X}La_XZn_{0.92}Nb_{1.5}O_{6.92}$ حيث تم تغيير تركيز اللانثانوم في مدى X= 0.10 - X= 0.22، وتبين من خلال تحليل حيود الاشعة السينية بان السيراميك ينمو منفردا وبحبيبات حجمها يزداد من 33 - 57 نانومتر عند زيادة تركيز اللانثانوم من 0.10 - 0.20، وتبين من خلال حيود الاشعة السينية في المدى الحراري 298 - 470 كلفن بان الاجهاد المايكرووي، كثافة الخلل وثابت البنية تزداد بازدياد درجة الحرارة بينما يتناقص حجم الحبيبة في النطاق 298 - 390 كلفن. بالاضافة الى ذلك، فان دراسة طيف الممانعة في حرارة الغرفة في مدى التردد 10 - 1800 ميجاهيرتز لتحديد طيف المواسعة، الموصلية، ثابت الانعكاس، درجة ضياع الموجة

الراجعة ونسبة الجهد الموقوف للداخل والتي تلزم لتحديد خصائص المادة كمرنان فعال في تكنولوجيا الاتصالات تتاثر بقوة بنسبة التطعيم بعنصر اللانثانوم، وقد تبين ان المواسعة تزداد من 13.50 - 20.60 ، بيكوفاراد عند زيادة كمية اللانثانوم من 0.10 - 0.22، وتبين ايضا بان ثابت العازلية النسبي يزداد من 31-55 بازدياد اللانثانوم من 0.10 - 0.20.